



Budapest University of Technology and Economics
Faculty of Electrical Engineering and Informatics
Department of Broadband Infocommunications and Electromagnetic Theory



Magnetic attitude controller for educational purposes

Student Name:
Supervisor:

Ainur Aman
Herman Tibor

2023

Contents

1	The Attitude Determination and Control System	4
1.1	Importance of ADCS	4
1.2	Small satellites ADCS	4
1.3	Magnetic torque attitude control	5
2	Magnetism	6
2.1	Magnetization	6
2.2	Magnetic hysteresis	6
2.3	Remanence	7
2.4	Hard iron and soft iron effects	8
3	Coil Design	9
3.1	Requirements	9
3.2	Coil making technology	10
3.3	Measurements	11
4	Prototype Design	17
4.1	Hardware Components and Specification	17
4.2	Block Scheme	18
4.3	Realized Prototype	20
5	Algorithm	21
5.1	Demagnetization	21
5.2	Calibration	22
5.3	Random excitation	22
5.4	Setup algorithm	22
5.5	Control algorithm	23
5.6	Functions	26
5.7	Source code for circuit testing	26

Összefoglaló

A kutatás témája egy oktatási célú, mágneses alapú helyzetstabilizáló rendszer tervezése, mely a BME Űrmérnök szakos hallgatói számára készült, akik laboratóriumi mérés során szerezhhetnek tapasztalatot a témában. Célja, hogy oktatási eszközként segítse az aktív helyzetstabilizálási elvek megértését és a hallgatók a gyakorlati tapasztalatot szerezzék a laboratóriumi mérések során.

A megvalósított eszköz két elektromágnesset, egy Raspberry Pi Pico mikrokontrollert, egy magnetométert és egy WiFi modult tartalmaz.

Abstract

This research project introduces a magnetic attitude controller specially designed for educational purposes, with a primary focus on enriching the learning experience within the Master's Aerospace Engineering program. The core objective is to develop a hands-on educational tool that facilitates a comprehensive understanding of attitude control principles and enables students to conduct practical test measurements. The objective is to design and implement a hardware controller utilizing two coils, a Raspberry Pi Pico microcontroller, a magnetometer, and a Wi-Fi module. The proposed system aims to provide a cost-effective and practical solution for small satellites, enabling educational institutions to enhance their satellite programs by incorporating attitude control capabilities.

Chapter 1

The Attitude Determination and Control System

The Attitude Determination and Control System (ADCS) is a system used on spacecraft to determine the orientation of the spacecraft in space and to control its orientation. The ADCS typically consists of sensors that measure the orientation of the spacecraft, control electronics that generate the appropriate control signals and actuators that generate the necessary forces or torques to control the orientation of the spacecraft. The ADCS is an important component of a spacecraft because the orientation of the spacecraft can affect its ability to perform its intended functions and remain stable in orbit.

1.1 Importance of ADCS

The Attitude Determination and Control System (ADCS) is essential for a spacecraft as its orientation in space directly impacts its functionality. For example, a satellite that is used for Earth observation may need to sustain a particular orientation to point its cameras at the Earth. Similarly, a satellite that is used for communication may need to keep a fixed orientation to point its antennas toward the Earth. In addition, the orientation of a spacecraft can affect its stability and its ability to withstand the forces of atmospheric drag and solar radiation pressure. An ADCS can help to ensure that a spacecraft can maintain a desired orientation to perform its intended functions and remain stable in orbit.

1.2 Small satellites ADCS

Several methods can be used for attitude determination and control of small satellites. Some common methods include:

Star trackers: These are optical sensors that can detect the position of stars in the sky, which can be used to determine the orientation of the satellite.

Sun sensors: These sensors can measure the direction of the sun, which can be used to determine the orientation of the satellite.

Gyroscopes: These sensors measure angular velocity, which can be integrated over time to determine the orientation of the satellite.

Magnetometers: These sensors measure the magnetic field of the Earth, which can be used to determine the orientation of the satellite.

Once the orientation of the satellite has been determined, control systems can be used to maintain or change its orientation. Some common control methods include:

Magnetic torque rods: These are small magnetic rods that can be used to generate torque on the satellite, which can be used to control its orientation.

Reaction wheels: These are small spinning wheels that can be used to generate torque on the satellite by changing their angular velocity.

Thrusters: These are small propulsion systems that can be used to generate a force on the satellite, which can be used to control its orientation.

1.3 Magnetic torque attitude control

Magnetic attitude control is a spacecraft control system that utilizes the Earth's magnetic field to regulate the orientation of the spacecraft. There are two primary types of magnetic attitude control: active and passive. In active magnetic attitude control, the spacecraft employs its magnetic field to interact with the Earth's magnetic field, enabling it to actively control its orientation. On the other hand, passive magnetic attitude control relies solely on the Earth's magnetic field to govern the spacecraft's orientation, without generating an independent magnetic field. This passive control can be achieved by utilizing a magnetic dipole, such as a permanent magnet, which naturally aligns itself with the Earth's magnetic field [1].

In this report, only the active ACS is discussed. Active magnetic torque attitude control is a type of control that uses magnetic fields to generate a torque, or rotational force, on the spacecraft. The magnitude and direction of the magnetic field can be adjusted to control the spacecraft's orientation.

The basic principle behind magnetic torque attitude control is simple. An asymmetric time-variable magnetic field is generated around the spacecraft using one or more magnetic coils. Changing the input current of the coil with the controller leads to a change in the electromagnetic field. This magnetic field interacts with the magnetic field of the Earth and generates a torque on the spacecraft. By adjusting the strength and orientation of the magnetic field, the spacecraft's attitude can be controlled. The control torque can be characterized as:

$$\mathbf{t}_{\text{mag}} = \mathbf{d} \times \mathbf{b} \quad (1.1)$$

where d - magnetic dipole moment, b - Earth's Magnetic field, t_{mag} - control torque.

In the case of picosatellites, which are small satellites with a mass of no more than 1 kg, magnetic torque control can be used to accurately and efficiently control the satellite's attitude.

One of the key advantages of using magnetic torque for attitude control is that it allows for a high degree of control and precision, even with very small satellites. This is because the magnetic fields generated by the satellite can be easily controlled and directed, allowing for precise control over the satellite's orientation.

Additionally, magnetic torque attitude control is a relatively low-power method of controlling a satellite's attitude, which is important for picosatellites, which typically have limited power available. In average picosatellites can produce $5 \times 10^{-1} \text{ W}$ - 2.5W, while magnetorquers consume maximum $1 \times 10^{-3} \text{ W}$ - 10^{-2} W of electric power. This makes it a good choice for controlling the orientation of picosatellites in space. [3]

Overall, magnetic torque attitude control is a useful tool for controlling the orientation of picosatellites in space, allowing for precise and efficient control even with very small and low-power satellites. However, the primary focus of this project is to design only a model for the magnetic attitude controller.

Chapter 2

Magnetism

2.1 Magnetization

Magnetization is a vector field that represents the density of both permanent and induced magnetic dipole moments within a material. The magnetic dipole moment arises from the movement of electrons. At the atomic level, electrons orbit the nucleus and spin around their axes, and the direction of the electron's magnetic moment aligns with its spin angular momentum. The sum of the orbital and spin magnetic moments of an atom results in its net magnetic moment. Some materials cannot be magnetized because the net magnetic moments cancel each other out. Based on their magnetization response, materials can be classified as diamagnetic, paramagnetic, or ferromagnetic. Diamagnetic materials weakly magnetize when an external magnetic field is applied. Paramagnetic materials can be magnetized only when an external magnetic field is present, and they return to their non-magnetized state when the field is removed. In contrast, ferromagnetic materials retain a significant portion of their net magnetic moment even after the external field is removed.

For diamagnetic and paramagnetic materials the relationship between magnetisation M and magnetic field H can be characterized as:

$$\mathbf{M} = \chi \times \mathbf{H} \quad (2.1)$$

where χ is magnetic susceptibility. However, this linear relationship is not true for ferromagnetic materials.

2.2 Magnetic hysteresis

Magnetic hysteresis is a phenomenon that occurs in ferromagnetic materials. Fig. 2.1 illustrates a hysteresis loop, which shows the relationship between magnetic flux density and the applied magnetic field. The dotted curve represents the initial magnetization curve, demonstrating how magnetic flux increases with the applied magnetic field until it saturates at point a. When the magnetic field is removed, the flux remains, which is known as remanence. To eliminate this remanence, a magnetizing intensity in the opposite direction is applied, reducing the flux to zero, a point known as coercivity. The curve continues as the magnetic field is applied until it reaches the saturation point. When the magnetic field is eliminated, remanent magnetization is still present but in the opposite direction. The magnetic field is then reapplied, and it returns to point a. This created hysteresis loop is a representation of the characteristics specific to ferromagnetic materials, providing a clear illustration of the relationship between magnetic flux density and the applied magnetic field.

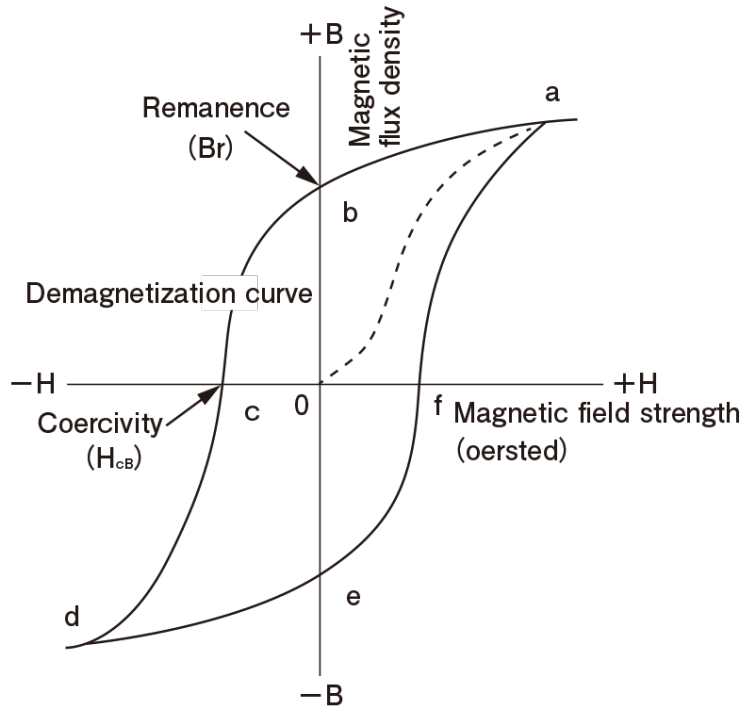


Figure 2.1: Magnetic hysteresis loop

2.3 Remanence

Remanent magnetization within the ferromagnetic core of an attitude controller can cause interference and compromise the reliability of the system. To ensure stable control and precise orientation of a satellite, it is critical to remove remanence. Demagnetization is the process by which this is achieved.

Demagnetization is the process of reducing or eliminating the remanent magnetization in a material, such as the ferromagnetic core of the attitude controller. This procedure is essential to maintain control and guarantee system functionality. There are several techniques used for demagnetization, depending on the specific requirements of the system.

Demagnetization can be achieved through thermal demagnetization, a process that involves heating the material to high temperatures. However, this method is not suitable for a satellite in space. Alternatively, the common method for demagnetization involves applying an alternating magnetic field, which gradually reduces the residual magnetization to nearly zero levels. In Fig. 5.1, it can be seen how applying an alternating magnetic field can effectively decrease remanence to almost zero. This is the strategy we will apply to this project.

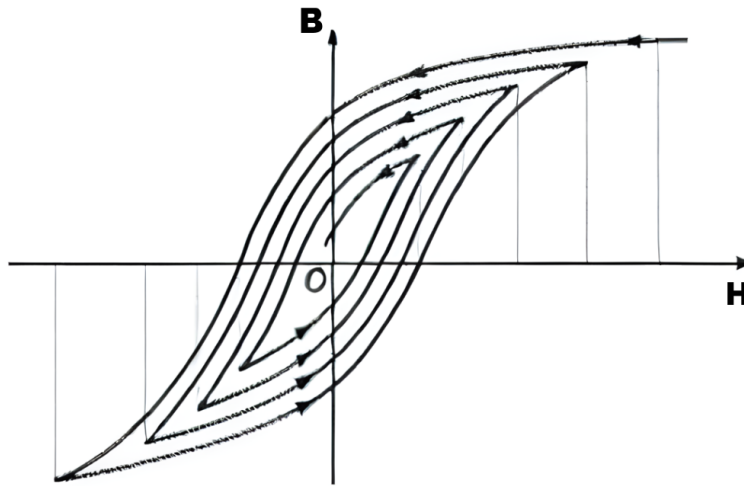


Figure 2.2: Demagnetization

2.4 Hard iron and soft iron effects

In a pursuit to achieve precise control and reliable performance other challenges related to external influences are hard iron and soft iron effects. One of the most notable disruptions in magnetometer readings is hard iron effects. These effects are primarily associated with stationary, magnetic noise sources, commonly originating from metallic objects close to the magnetometer on the circuit board. The distinctive characteristic of hard iron effects is their ability to shift the origin of the ideal sphere that magnetometer measurements should ideally adhere to. When these effects are present, our readings deviate from the anticipated ideal behavior.

Another class of disturbances that impact magnetometer performance is known as soft iron effects. These effects are more subtle and stem from objects near the sensor that distort the surrounding magnetic field. Unlike hard iron effects that cause shifts in the origin of the ideal sphere, soft iron effects result in the stretching and tilting of the ideal measurement sphere. The output readings are not spherical; instead, they conform to an ellipsoid shape.

In dealing with the challenges posed by hard iron effects and soft iron effects in magnetometer readings, calibration techniques are employed. Correcting for hard iron offset is a relatively straightforward process that involves adding or subtracting a fixed value from the magnetometer measurements. On the other hand, soft iron effects are more complex, distorting the ideal measurement sphere. As a result, we prioritize the correction of hard iron offset due to its simplicity and significant impact on measurement accuracy.

Chapter 3

Coil Design

This chapter discusses the steps of building the coil required for the circuit. First, the requirements of the coil are discussed. Secondly, calculations are made. Thirdly, the necessary components are chosen, and the coil-making technology is described in detail. Throughout the process, the approach used is defined, and the important decisions to consider during design are pointed out.

3.1 Requirements

The most important requirements for magnetorquer design are the core, the wire diameter, and the number of turns. These decisions affect magnetic dipole, operative region, and power consumption.

The core choice for the design of a magnetorquer can be between paramagnetic and ferromagnetic materials. However, since our goal is to achieve a highly induced magnetic field and to provide a more comprehensive approach to understanding the process of designing this magnetorquer, the decision is to select a ferromagnetic material. Due to its combination of desirable properties, such as moderate permeability, high flux density, and cost-effectiveness, the iron core was chosen as an excellent option for the design of our model. 3.1 [12]

	Sensitivity (permeability)	Strength (flux density)	Cost
Highest	Nickel-Iron	Iron-Cobalt	Iron-Cobalt
	Silicon Iron	Iron	Nickel-Iron
	Iron	Silicon Iron	Ferritic Stainless
	Iron-Cobalt	Ferritic Stainless	Silicon Iron
Lowest	Ferritic Stainless	Nickel-Iron	Iron

Figure 3.1: Magnetic alloy selection matrix

For optimum power efficiency and torque, a wire diameter of 0.2mm was chosen, considering the least amount of power required. Additionally, the wire was coated with enamel insulation, which added a thickness of 0.04mm. This specific combination of a 0.2mm wire and 0.04mm

enamel insulation provided excellent electrical insulation properties while maintaining a compact wire diameter. With the coil body and wire diameter determined, the number of turns was recalculated, taking into account the requirement for bifilar winding 3.2. A total of 860 turns ($N=860$) were calculated for this coil. The wire has a diameter of 0.24mm, the coil body has an inner diameter of 10.3mm, and the inner length of the coil is 30.7mm.

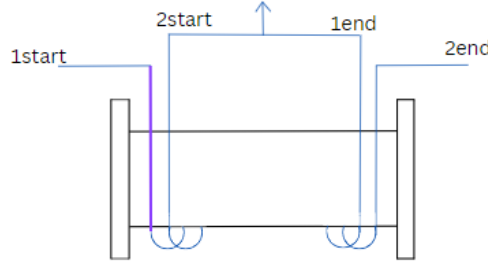


Figure 3.2: Coil Design

3.2 Coil making technology

After finalizing the circuit design, the coil design process was initiated. In this case, a top-to-bottom approach was adopted, considering the dimensional and mass limitations typically associated with satellite devices. The circuit with dimensions of 10*10 cm was initially designed, and suitable space was allocated for the coils accordingly. Based on the allocated space, an appropriate iron core was chosen for the coil, and in this prototype. To prevent short circuits between the coil wire and the iron core, a 3D program called Onshape was utilized to design the body of the coil. The coil body also needed to facilitate winding using a coil winding machine in the lab. A 3D design screenshot of the coil body is presented in Fig. 3.3. After 3D printing the coil body, it is important to note that the main core and upper cup of the core were printed separately, and they needed to be joined into a single piece for use in the machine Fig. 3.4. Therefore, they were glued together, resulting in a slight decrease in the length of the coil body compared to the pre-calculated length.

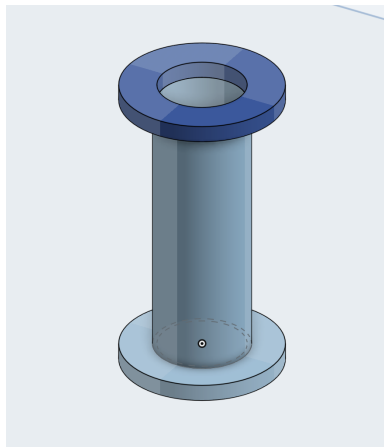


Figure 3.3: 3D Design of Coil Body

After preparing the coil body and selecting the wire, the actual winding process commenced, taking into account important considerations in coil winding technology. Firstly, a small hole was drilled in the coil body to secure the wire initially, which corresponds to the "Wire1Start"

and "Wire2Start" points labeled in the schematic diagram of the circuit. Prior to beginning the winding process, Kapton paper was applied as an insulating material on the first layer and after every subsequent wire layer. However, it's important to note that the Kapton paper, with its 0.03mm thickness, reduced the available space for winding by 0.48mm when multiplied by the 16 rows. Consequently, this affected the total number of turns that could be accommodated. As a result, the final number of turns achieved was: First coil number of turns: 772; Second coil number of turn: 740;

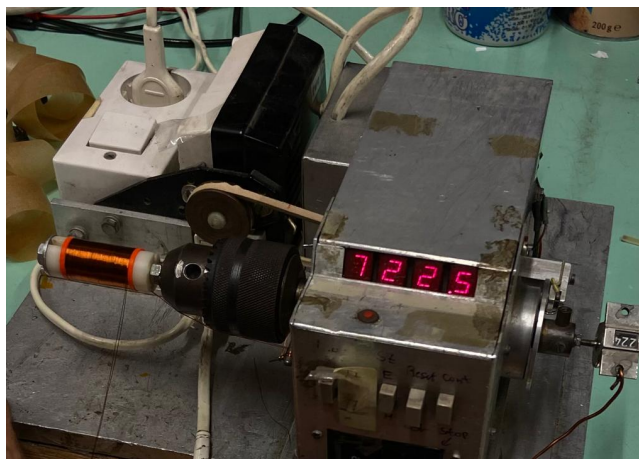


Figure 3.4: Coil Winding Machine

3.3 Measurements

Initially, we conducted measurements to determine the impedance and phase characteristics of the coils within a frequency range of 20Hz-1MHz. Using these results, we plotted the corresponding graphs in MATLAB. Although physically there are two coils, we performed measurements for four coils due to the utilization of bifilar winding in each coil, effectively treating Wire1 and Wire2 as separate coils within the same coil body. Specifically, the first coil, C722, encompasses Wire1 and Wire2 as two coils embedded in a single coil body. This same configuration applies to the C740 coil. The objective of these measurements was to ensure that the characteristics of all four coils were identical. As illustrated in Fig. 3.5, the impedance and phase characteristics of all four coils exhibited remarkable similarity.

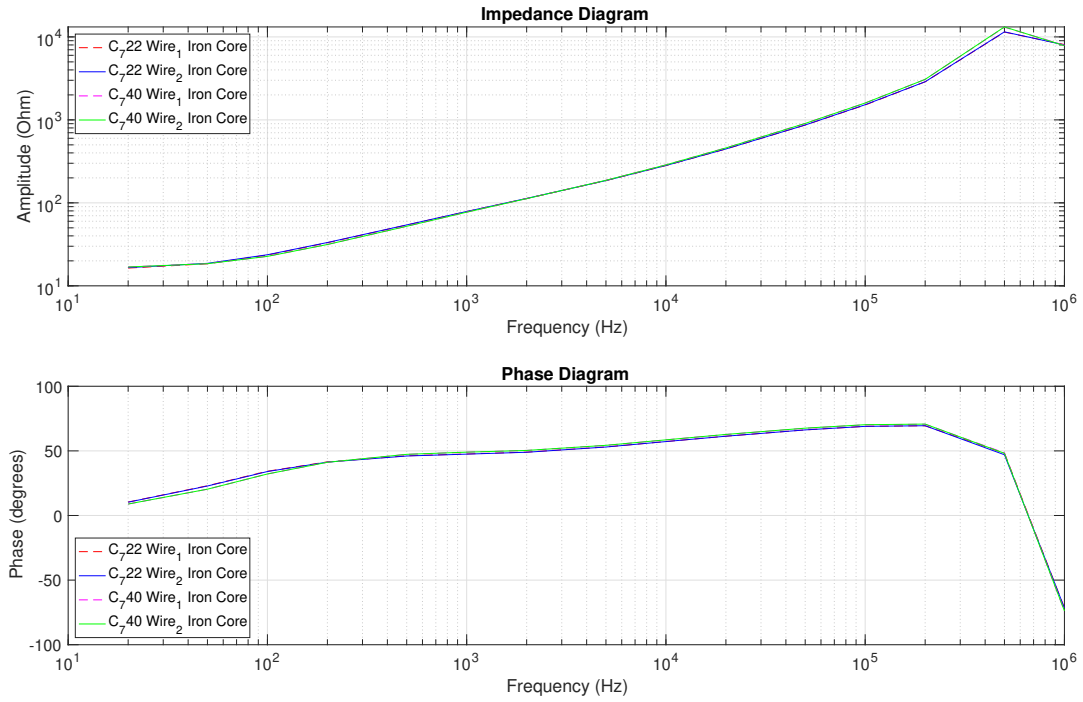


Figure 3.5: Characteristics of all coils

Fig. 3.8 illustrates the measurement setup employed to measure the current and time constant of the coil. A 3.3 Ohm resistor was connected in series with the coil. The frequency and duty cycle were controlled using the code 5.7. The voltage across an RL circuit during the charging phase can be mathematically described by the equation:

$$V(t) = V_0 \cdot (1 - e^{-\frac{t}{\tau}}) \quad (3.1)$$

where τ represents the time constant.

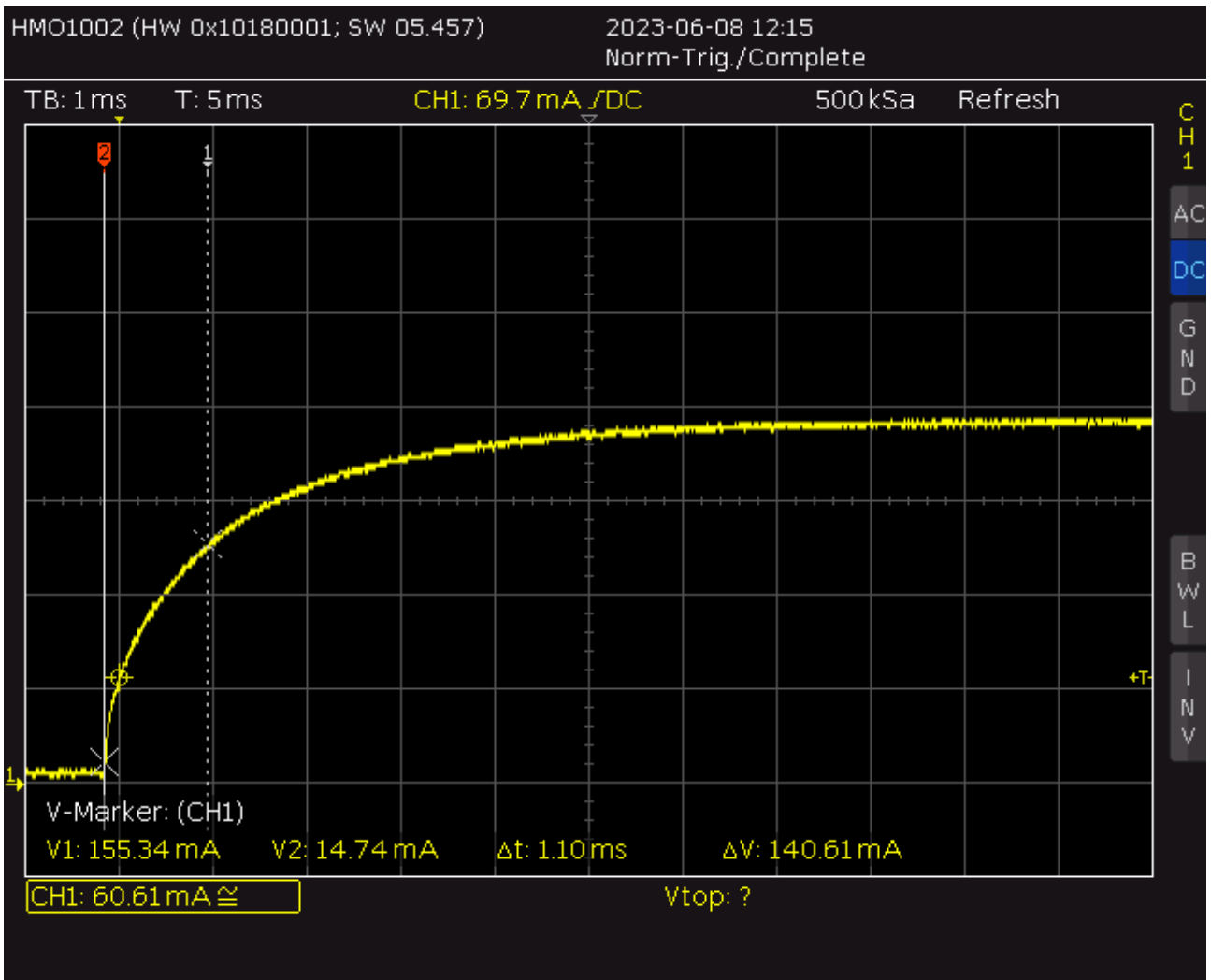


Figure 3.6: Time constant of the coil

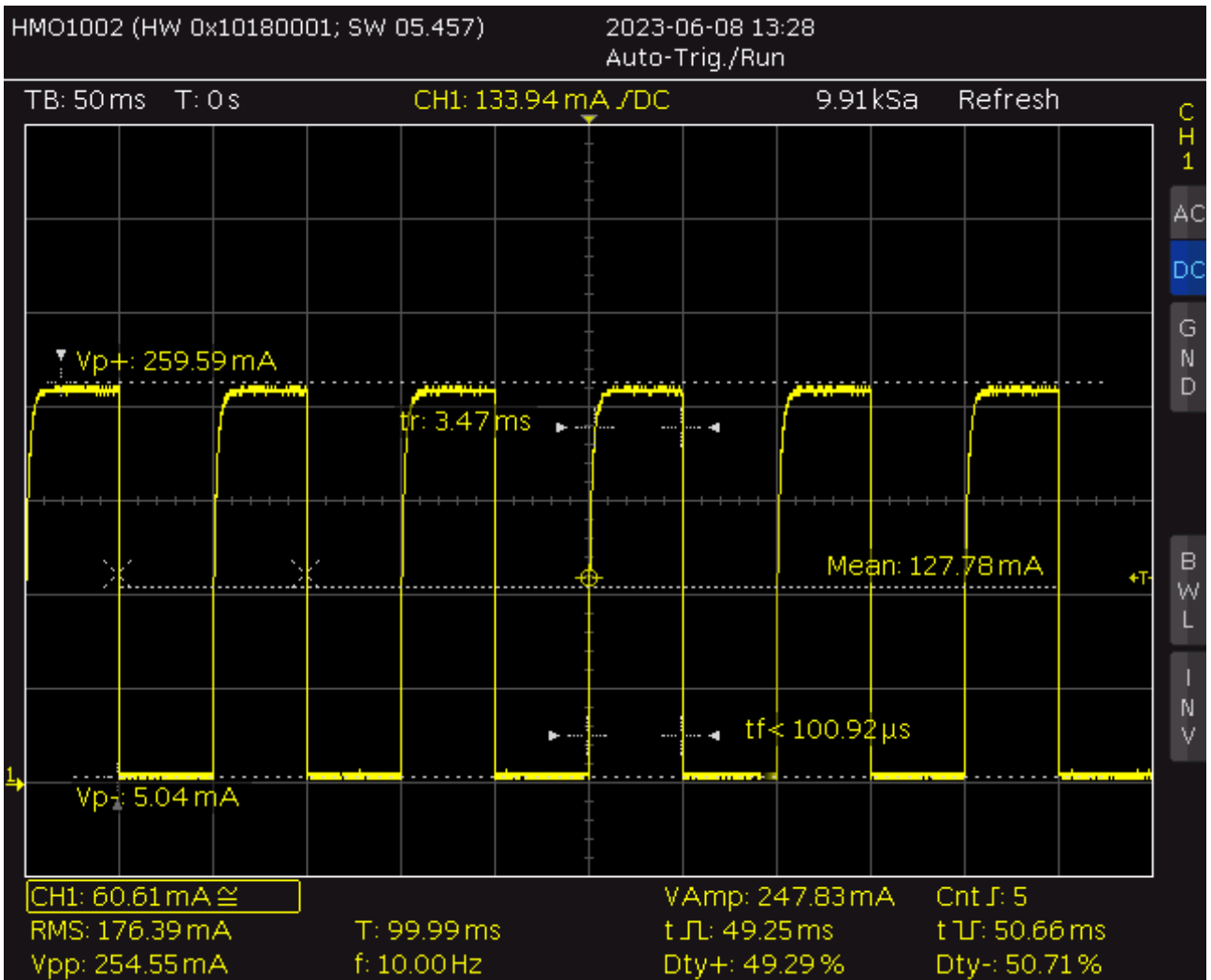


Figure 3.7: 10Hz signal

In Fig. 3.6, the voltage exhibits an exponential rise towards its maximum value, V_0 . Consequently, the time constant τ in Fig. 3.6 signifies the duration for the voltage to reach 63.2%

$$(1 - e^{-\frac{t}{\tau}}) \quad (3.2)$$

of its maximum value. Therefore, by observing the graph, we identified the time point at which the voltage reaches 63.2% of its maximum value and determined the corresponding time value τ at this point, which is 1.1ms, as evident in Fig. 3.6. Since we measured the time constant and resistance of the coil which is 16 Ohm, we can derive inductance L of the coil which is 17.6 mH.

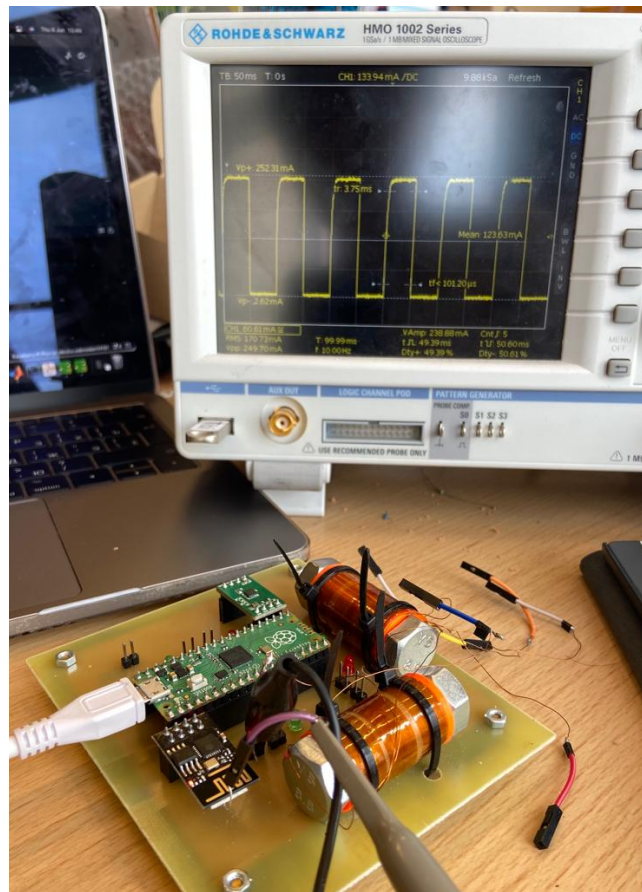


Figure 3.8: Measurement Setup

Also, in Figure 3.7, the mean current can be observed when a 10Hz signal with a 50% duty cycle is applied. To analyze the relationship between the duty cycle and the mean current, measurements were conducted across the range of 0-100% duty cycle, and a graph depicting the current as a function of the duty cycle was plotted (see Figure 3.9). The graph clearly shows a linear dependence between the current and the duty cycle, as an increase in the duty cycle results in a proportional increase in the current.

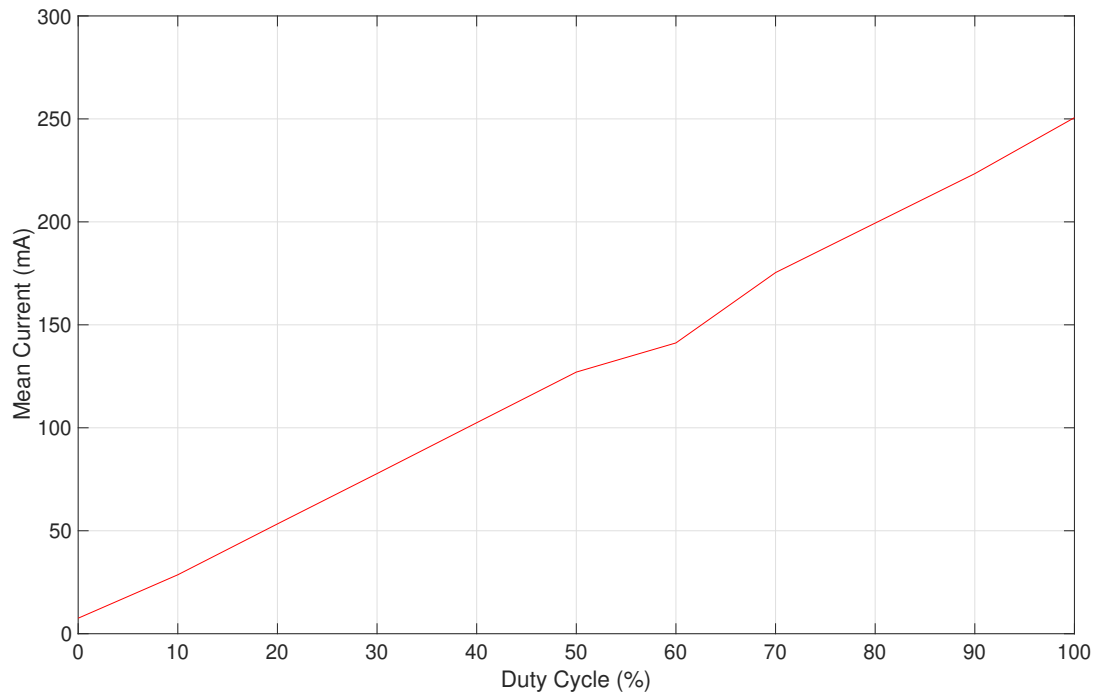


Figure 3.9: Relationship between Duty Cycle and Mean Current

Chapter 4

Prototype Design

This chapter discusses the steps of building the prototype of the attitude control system. First, the necessary hardware components are selected. Secondly, a schematic and layout of the PCB are designed. Thirdly, the circuit is printed, and all necessary components are mounted. Throughout the process, the approach used is defined, and the important decisions to consider during design are highlighted.

4.1 Hardware Components and Specification

For this project, the simplicity and availability of components was a priority. The chosen setup involves utilizing the Raspberry Pi Pico microcontroller with datasheet [4] in conjunction with a MOSFET to control the power delivered to the coil through Pulse Width Modulation (PWM).

This approach allows us to run our control software on the microcontroller, which in turn generates a varying current through the coil, thereby creating the desired magnetic field for control purposes. One crucial consideration was the ability to control the current in both forward and reverse directions to maintain controllability. That is why the coil is specifically designed considering such a goal.

4.2 Block Scheme

The circuit was designed in KiCad - [9].

In Fig.4.1 we can see the Block Scheme of the schematic diagram of the circuit.

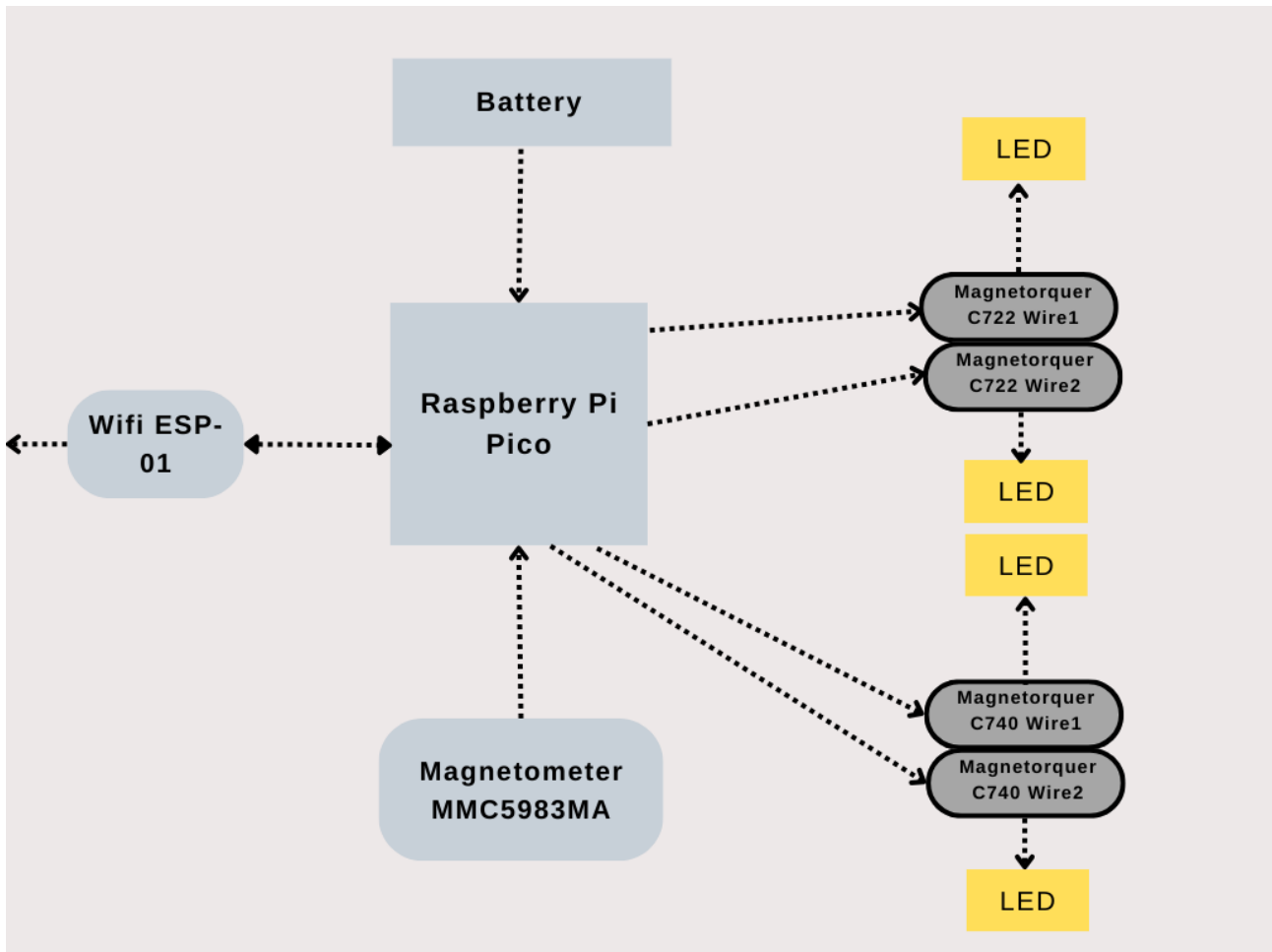


Figure 4.1: Block Scheme

The Raspberry Pi Pico microcontroller is utilized to control the circuit. During the design of the circuit, the GPIO pin selection in the microcontroller for PWM should be carefully considered according to the data sheet [4]. The table 4.2 in the data sheet shows the specific combinations of GPIO pins that can not be controlled independently. Choosing those pins will compromise the functionality of the system.

4.5.2. Programmer's Model

All 30 GPIO pins on RP2040 can be used for PWM:

Table 514. Mapping of PWM channels to GPIO pins on RP2040. This is also shown in the main GPIO function table, Table 278

GPIO	0	1	2	3	4	5	6	7	8	9	10	11	12	13	14	15
PWM Channel	0A	0B	1A	1B	2A	2B	3A	3B	4A	4B	5A	5B	6A	6B	7A	7B
GPIO	16	17	18	19	20	21	22	23	24	25	26	27	28	29		
PWM Channel	0A	0B	1A	1B	2A	2B	3A	3B	4A	4B	5A	5B	6A	6B		

Figure 4.2: PWM table

Positioned in the middle top section is the battery, accompanied by a circuit designed for reverse polarity protection.

On the right side, two magnetorquers can be observed. The 'C' represents the coil, and the number denotes the number of turns in each of the coils. However, it's important to note that physically, there is only one coil with a bifilar winding. The reason for using two separate coils in the block scheme is due to its application. The bifilar winding involves two wires wound together on one core, and the controller activates only one transistor at a time to generate a magnetic field in a specific direction. Previously, a circuit with a single magnetorquer used an H-bridge configuration, which required four transistors and controlled activation of two of them.

In yellow, four LEDs serve the purpose of indicating the current flow in the coil in a specific direction.

The MMC5983MA magnetometer is employed to measure the generated magnetic field and provide feedback to the controller for appropriate action. The ESP-01 WiFi module is situated, facilitating the transmission of data measured by the magnetometer.

4.3 Realized Prototype

The realized PCB can be seen in Fig. 4.3 and in Fig. 4.4.



Figure 4.3: Realized prototype Front side

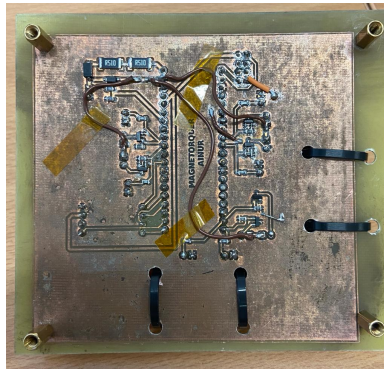


Figure 4.4: Realized prototype Back Side

Components:

- Raspberry Pi Pico,
- Iron core coil,
- NMOS MOSFET YJL05N04A
- WIFI ESP-01
- Magnetometer MMC5983MA
- Three red and three green LEDs

Chapter 5

Algorithm

This chapter discusses the steps for writing a setup and attitude control algorithm. First, we ensure measurement accuracy by correcting any offsets and addressing residual magnetization. Second, we calculate the current orientation of the controller. Third, we rotate the device to the target orientation.

5.1 Demagnetization

To eliminate remanent magnetization, a demagnetization function is applied using an alternating magnetic field on the coils. PWM is used to control the intensity of the alternating magnetic field. By adjusting the duty cycle and frequency of the PWM signal, you can precisely regulate the magnetic field's strength. A higher duty cycle corresponds to a stronger magnetic field, while a lower duty cycle results in a weaker magnetic field. The frequency of the PWM signal can also affect the smoothness and efficiency of the demagnetization process. As illustrated in Fig. 5.1, decreasing the PWM duty cycle reduces the magnetic field strength. The alternating magnetic field, when applied in this controlled manner, steadily weakens any remanent magnetization in the material until it approaches zero.

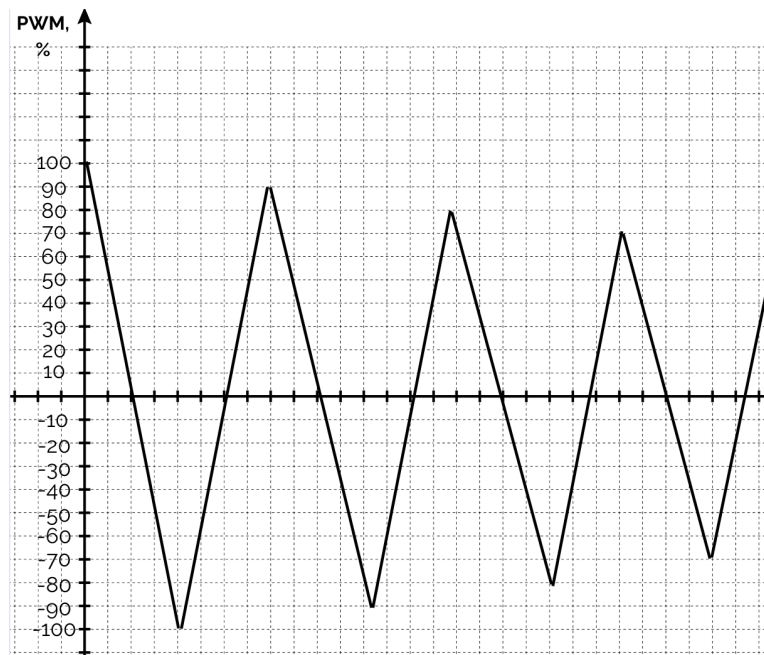


Figure 5.1: Demagnetization

5.2 Calibration

The calibration process plays an important role in ensuring accurate and reliable magnetometer measurements. The calibration technique applied in this project uses mathematical approximations, particularly involving inverse trigonometric functions [11]. This approach calculates the hard iron offset from measured data.

To compute hard iron offset the calibration library was used which provides functions to initialize, update, calculate, and get calibration results. First, the calibration should be initialized with a sophisticated function. This function initializes various variables and matrices that will be used during the calibration process[11].

The sensor performs measurements and passes the data to the update calibration function, which is responsible for iteratively performing calculations with incoming data and accumulating the values into previously initialized matrices.

Calculate calibration result function performs operations on matrices and computes hard iron offset, which can be retried using get calibration result. Hence, the calibration values are stored in a matrix and used to correct further measurements.

5.3 Random excitation

A random excitation test is conducted to verify the effectiveness of the demagnetization and calibration processes. The goal is to assess whether the magnetic field measurements, after applying demagnetization and calibration, yield results consistent with measurements taken both before and after the procedures. This test helps ensure that the device's magnetometer operates reliably and consistently by comparing the values obtained during various phases of the testing process. It is used as a quality control step to confirm that the demagnetization and calibration have successfully mitigated any residual magnetization or other sources of error, ultimately leading to accurate and reliable measurements.

5.4 Setup algorithm

Fig. 5.2 illustrates how the setup algorithm should function by combining previously discussed functions. First, to remove remanent magnetization demagnetization is applied. After calibration function ensures that the hard iron offset is calculated and removed for every subsequent measurement. During the continuous measurement, random excitation can be applied to verify whether demagnetization and calibration are applied correctly and whether the measurements are accurate. It is important to note that the calibration function is set in the beginning and remains constant because it is expected to remain valid under stable conditions. In contrast, demagnetization and random excitation are applied before each measurement, ensuring that the system is free from interference and that the measurements accurately reflect the system's state at that moment.

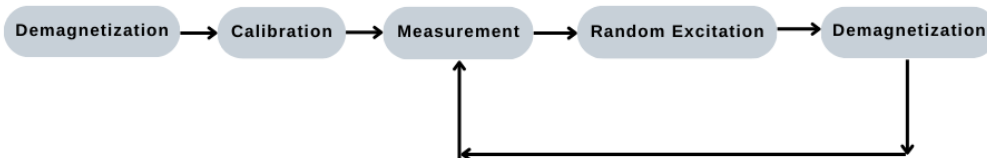


Figure 5.2: Setup algorithm

5.5 Control algorithm

- Read the magnetometer data continuously
- Calculate the current orientation based on the magnetic field data
- Set the target
- Calculate control signal
- Adjust the coil to rotate the device to the target orientation according to the control signal

Assuming the magnetometer is calibrated and set correctly to continuously read the data, the control algorithm is initiated. The requirements for the control algorithm include the ability to orient itself around one axis. To achieve this, the first step is to determine the current orientation of the device. Since the goal is to change the attitude along one axis, one of the vectors in the selected plane can be considered as the reference vector to calculate the bearing angle, which represents the orientation of the controller. Once the orientation is determined, the target orientation can be received as an input parameter. Taking into account the field vector, bearing angle, and target orientation, the control function should be capable of computing control signals for the coil to orient itself in the direction of the target vector. It is important to note that at the time of writing this report, the control algorithm is still in development, and therefore, a detailed discussion of its functionality is not included.

Conclusion and Future Work

This research project has introduced a magnetic attitude controller, designed for educational purposes. The primary goal was to create a hands-on educational tool that not only assists in understanding attitude control principles but also equips students with the ability to perform practical test measurements. This approach ensures that the subject of attitude determination and control can be effectively taught, allowing students to interact with the controller model in a manner that demonstrates essential concepts of magnetic torque attitude control systems. Moreover, the project utilized affordable and available hardware components, making this controller prototype easy to design and integrate into educational programs for institutions.

The current report discussed the design, measurements, and correct setup of the hardware controller, as well as the underlying theory necessary for a comprehensive understanding of the device's design and functionality. However, the ongoing development of the control algorithm represents the next phase of this research project. The control algorithm is a critical component that will enable the system to effectively orient itself, making it a complete and functional magnetic attitude controller. Future work will focus on refining and optimizing the control algorithm to ensure reliable orientation control.

Bibliography

- [1] Progress in Aerospace Sciences 109 (2019) 100546 2.
- [2] J.R. Wertz. *Spacecraft Attitude Determination and Control*. Dordrecht: D.Reidel Publishing Co., 1978.
- [3] A. Colagrossi and M. Lavagna. "Advances in Space Research 62" (2018): 3383–3397.
- [4] Raspberry Pi Ltd. RP2040 Datasheet (2021), p. 524. Retrieved from <https://datasheets.raspberrypi.com/rp2040/rp2040-datasheet.pdf>. Accessed November 2, 2023.
- [5] Purcell, E. M., & Morin, D. J. (2013). *Electricity and Magnetism* (3rd ed.). Cambridge University Press.
- [6] Griffiths, D. J. (2017). *Introduction to Electrodynamics* (4th ed.). Cambridge University Press.
- [7] Simons, L. E. (2019). "Helmholtz Coils." In *Encyclopedia of Geomagnetism and Paleomagnetism* (pp. 589-590). Springer.
- [8] Uzunovic, A., & McAlpine, A. (2019). "Design of Helmholtz Coils for Magnetic Field Generation." In *2019 IEEE Texas Power and Energy Conference (TPEC)* (pp. 1-6). IEEE.
- [9] KiCad. Retrieved from <http://kicad-pcb.org/>. Accessed November 2, 2023.
- [10] Onshape. Retrieved from <https://www.onshape.com/en/>. Accessed November 2, 2023.
- [11] <https://www.nxp.com/docs/en/application-note/AN5019.pdf>
- [12] L. L. Harner, «A Simplified Method of Selecting Soft Magnetic Alloys,» Carpenter Technology Corporation, May 1999.<https://www.carpentertechnology.com/blog/a-simplified-method-of-selecting-soft-magnetic-alloys>

Appendix

5.6 Functions

5.7 Source code for circuit testing

The source code for testing the circuit is : 5.7.

```
int C722_Start1 = 6;
int C722_End2 = 7;
int C740_Start1 = 14;
int C740_End2 = 15;

void setup() {
  pinMode(C722_Start1, OUTPUT);
  pinMode(C722_End2, OUTPUT);
  pinMode(C740_Start1, OUTPUT);
  pinMode(C740_End2, OUTPUT);
  digitalWrite(C740_Start1, LOW);
  digitalWrite(C740_End2, LOW);
  digitalWrite(C722_End2, LOW);
  digitalWrite(C722_Start1, LOW);
}
int x = 50;
void loop() {
  digitalWrite(C722_Start1, HIGH);
  delay(x);
  digitalWrite(C722_Start1, LOW);
  delay(100-x);
}
```

Listing 5.1: Calibration function

```
void calibrateSensor() {
  for (int i=0; i<3; i++)
    Bp_cal[i] = 0;
  MagSensorInitCalibration();
  for(int i = 0; i < 10; i++){
    float Bp[4]={0,0,0,1.0};
    T_MATRIX scaledX, scaledY, scaledZ;
    readAndScaleData(scaledX, scaledY, scaledZ);
    Bp[0] = scaledX;
```

```

        Bp[1] = scaledY;
        Bp[2] = scaledZ;
        MagSensorUpdateCalibration(Bp);
        delay(random(500,1000));
    }
    MagSensorCalculateCalibrationResult();

    Serial.println(MagSensorGetCalibrationResult(Bp_cal));
}
}

```

Listing 5.2: Function to calculate orientation angle

```

float calculateOrientationAngle() {
    float bearingAngleRad = atan2(Bp[1], Bp[0]);
    float bearingAngleDeg = bearingAngleRad * 180 / M_PI;
    return bearingAngleDeg;
}

```

List of Figures

2.1	Magnetic hysteresis loop	7
2.2	Demagnetization	8
3.1	Magnetic alloy selection matrix	9
3.2	Coil Design	10
3.3	3D Design of Coil Body	10
3.4	Coil Winding Machine	11
3.5	Characteristics of all coils	12
3.6	Time constant of the coil	13
3.7	10Hz signal	14
3.8	Measurement Setup	15
3.9	Relationship between Duty Cycle and Mean Current	16
4.1	Block Scheme	18
4.2	PWM table	19
4.3	Realized prototype Front side	20
4.4	Realized prototype Back Side	20
5.1	Demagnetization	21
5.2	Setup algorithm	22